Organic & Biomolecular Chemistry

ROYAL SOCIETY OF CHEMISTRY

COMMUNICATION

View Article Online
View Journal

Cite this: DOI: 10.1039/d2ob00357k

Received 21st February 2022,
Accepted 4th March 2022

DOI: 10.1039/d2ob00357k

rsc.li/obc

Tetraphenylethylene–DNA conjugates: influence of sticky ends and DNA sequence length on the supramolecular assembly of AIE-active vesicles†

Simon Rothenbühler,[a] Adrian Gonzalez,[a] Ioan Iacovache,[b] Simon M. Langenegger,[a] Benoît Zuber[b] and Robert Häner[a]

The supramolecular assembly of DNA conjugates, functionalized with tetraphenylethylene (TPE) sticky ends, into vesicular structures is described. The aggregation-induced emission (AIE) active TPE units allow monitoring the assembly process by fluorescence spectroscopy. The number of TPE modifications in the overhangs of the conjugates influences the supramolecular assembly behavior. A minimum of two TPE residues on each end are required to ensure a well-defined assembly process. The design of the presented DNA-based nanostructures offers tailored functionalization with applications in DNA nanotechnology.

Programmability and reversibility of nucleic acid hybridization are key attributes for the construction of well-defined DNA nanostructures in the rapidly evolving field of DNA nanotechnology.[1–8] The assembly of sticky end containing DNA represents an alternative approach to the well-known DNA origami strategy for the creation of nucleic acids nanostructures.[9–14] The presence of sticky ends enables the cohesion between DNA units which, in turn, can induce the assembly of nanosized supramolecular architectures.[15–17] The chemical and structural diversity of oligonucleotides, and therefore the associated applicability, is limited when solely the four canonical nucleotides are present.[18] Structures assembled from chemically modified oligonucleotides expand the scope of applications beyond the function of DNA in a purely biological context.[19–28] DNA-functionalized supramolecular polymers composed of DNA conjugates exhibit promising features that may be relevant in the fields of nanotechnology and the materials sciences.[29–37] Recently, we reported the supramolecular assembly of 3′-end modified DNA conjugates into vesicular constructs, either using phenanthrene or TPE sticky ends.[38,39] The polyamine spermine was found to be required for the formation of the DNA-constructed vesicles, as the coulombic repulsion between the negatively charged DNA backbones need to be neutralized for a successful assembly. In addition to spermine-mediated interactions between DNA duplexes, the supramolecular assembly process also depends on the hydrophobic interactions of the sticky ends. In the case of TPE incorporation into the oligonucleotides, AIE-active supramolecular assemblies are constructed. The development of AIE[40] has greatly stimulated the advancement of fluorescent supramolecular polymers composed of AIE active bioconjugates for biomedical, biosensing, or bioimaging applications.[41–48]

Herein, we present DNA-based vesicular constructs assembled from 3′-/5′-end modified TPE–DNA conjugates. The effect of different DNA conjugate designs on the nucleation temperature was studied by fluorescence-monitored annealing curves. The resulting nanostructures were visualized by atomic force microscopy (AFM) and cryo-electron microscopy (cryo-EM).

The DNA duplexes **1–5** investigated in this study are outlined in Fig. 1. The preparation of all TPE-modified oligonucleotides was carried out according to published procedures[39] *via* solid-phase synthesis using phosphoramidite chemistry and subsequent HPLC purification. The length of the sticky ends varies from one to three TPE units (duplexes **1–3**) in a 20-mer DNA. This set aims at the investigation of the influence of the hydrophobic TPE interactions on the supramolecular assembly behavior. In addition, the length of the DNA part was varied between 15 and 25 nucleotides with a constant length of three TPE sticky ends (duplexes **3–5**). Alterations within the DNA sequences were introduced in the center of the DNA strands in order to avoid changes at the TPE-modified ends of the duplex. The series of duplexes **3–5** serves the study of the dependence of the spermine-related interaction between DNA duplexes of different length.

A representative absorption spectrum of TPE-modified DNA duplexes is depicted in Fig. 2a and shows two distinct bands. The band centered around 260 nm originates from the combined absorption of DNA nucleobases and the TPE chromophores, whereas the band around 330 nm is due to TPE

[a]Department of Chemistry, Biochemistry and Pharmaceutical Sciences, University of Bern, Freiestrasse 3, CH-3012 Bern, Switzerland. E-mail: robert.haener@unibe.ch; http://www.haener.dcbp.unibe.ch
[b]Institute of Anatomy, University of Bern, Baltzerstrasse 2, CH-3012 Bern, Switzerland

†Electronic supplementary information (ESI) available: General methods, DNA conjugates synthesis, UV-Vis and fluorescence spectra, AFM, DLS, and cryo-EM images. See DOI: 10.1039/d2ob00357k

Duplex	Sequence
1	(TPE)-CTT CCT TGC ATC GGA CCT TG-(TPE) 3′-GAA GGA ACG TAG CCT GGA AC-5′
2	$(TPE)_2$-CTT CCT TGC ATC GGA CCT TG-$(TPE)_2$ 3′-GAA GGA ACG TAG CCT GGA AC-5′
3	$(TPE)_3$-CTT CCT TGC ATC GGA CCT TG-$(TPE)_3$ 3′-GAA GGA ACG TAG CCT GGA AC-5′
4	$(TPE)_3$-CTT CCT TGG ACC TTG-$(TPE)_3$ 3′-GAA GGA ACC TGG AAC-5′
5	$(TPE)_3$-CTT CCT TGC ACT GAA TCG GAC CTT G-$(TPE)_3$ 3′-GAA GGA ACG TGA CTT AGC CTG GAA C-5′

TPE =

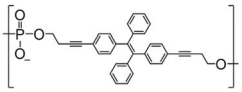

Fig. 1 DNA sequences of duplexes **1–5** and structure of the TPE building block.

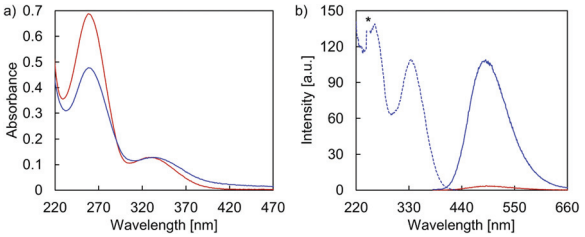

Fig. 2 (a) Temperature-dependent absorption spectra of **3**. (b) Temperature-dependent fluorescence emission (solid line) and excitation (dotted line) spectra of **3**. Conditions: 1 μM **3**, 10 mM sodium phosphate buffer pH 7.2, 0.1 mM spermine·4 HCl, 20 vol% ethanol at 75 °C (red) and 20 °C after thermally controlled (0.5 °C min^{-1}) assembly process (blue), $\lambda_{ex.}$: 335 nm, $\lambda_{em.}$: 490 nm, * indicates a second-order diffraction.

absorption only. Upon controlled cooling from 75 °C to 20 °C, hypochromicity is observed at 260 nm, along with a bathochromic shift of the maximum from 327 nm to 332 nm. This temperature-dependent spectroscopic observation indicates for aggregation. The AIE behavior of **3** is exemplified by temperature-dependent fluorescence emission spectra, shown in Fig. 2b. Upon TPE excitation at 335 nm, emission is negligible at 75 °C suggesting no aggregation at this temperature. At 20 °C, however, an intense emission band centered around 490 nm is observed, which implies aggregation, detectable due to the fluorescent TPE chromophores. Comparable spectroscopic characteristics were observed for all other TPE-modified duplexes (Fig. S8–S11, ESI†).

AFM imaging (Fig. 3) was conducted to investigate the morphology of the supramolecular assemblies after performing a thermally controlled assembly procedure, which involved the cooling of the solution from 75 °C to 20 °C with a gradient of 0.5 °C min^{-1}. In a first set of experiments, the influence of the length of the TPE overhangs on the morphology of the self-assemblies was examined (duplexes **3**, **2**, and **1**). Single and agglomerated vesicular aggregates with a height of up to 40 nm were observed for **3** on APTES-modified mica. (Fig. 3a, Fig. S12, ESI†). Assembly of **2**, which is shortened at the sticky ends by one TPE unit, also led to the formation of vesicles (**2**, Fig. 3b). These vesicles occurred, in contrast to the ones formed by **3**, as single vesicles, *i.e.*, not as agglomerates. Compared to duplex **3**, the size range of the supramolecular assemblies composed of **2** increased to a height of about 80 nm and a diameter of up to 150 nm (Fig. S13, ESI†). The deflection scan at the bottom of Fig. 3 further illustrates the vesicular nature of the supramolecular assemblies. To complement AFM imaging by a solution-based method, dynamic light scattering (DLS) experiments of non-agglomerated vesicles assembled from **2** were conducted. An average diameter of 235 ± 59 nm was obtained (Fig. S17, ESI†). This is somewhat larger than the size range observed by AFM, however, considering that DLS monitors the hydrodynamic diameter of the vesicles, the two values are in good agreement. In contrast to duplexes **3** and **2**, duplex **1** bearing only one TPE moiety on each side of the duplex, did not form any observable structures (Fig. S14, ESI†). Fluorescence-monitored annealing curves further support the observations obtained from AFM experiments (Fig. 4a). In agreement with the AIE concept, TPE emission amplifies during the thermal assembly process, except for **1**. The temperature at which a sharp increase in fluorescence is detected, is denoted as the fluorescence onset temperature, and indicates the nucleation temperature and, thus, the start of the supramolecular assembly process. The absence of any discernible onset temperature for **1** is additional evidence that no nanosized aggregates are formed. A fluorescence onset temperature of 53 °C was determined for **2**. In contrast to **2**, duplex **3** does not exhibit a similarly sharp increase in fluorescence and, accordingly, a nucleation temperature range (60–62 °C) can be determined (Table 1). This trend demonstrates that extending the TPE sticky ends raises the nucleation temperature, which is explained by increased hydrophobic interactions between the overhangs. Accordingly, a minimum length of 2 TPE units per sticky end is required to ensure the supramolecular assembly of this type of DNA conjugates into vesicular nanostructures.

In a second set of experiments, the influence of the length of the DNA part on the morphology of the supramolecular assemblies was investigated by AFM (duplexes **3**, **4**, and **5**). Aggregates assembled from the 15-mer DNA **4** or 25-mer DNA **5** (Fig. 3c and d) show predominantly agglomerated vesicular structures, with heights of about up to 30 nm.

Hence, varying the length of the DNA part (within the scope of this study) does not have such a significant influence on the nanostructures as when the number of the TPEs in the overhangs is altered. This is also confirmed by fluorescence-monitored annealing curves (Fig. 4b). The nucleation temperature range for duplex **4** was measured to be 62–64 °C and the nucleation temperature for **5** was 56 °C. Together with the value obtained for duplex **3**, these three duplexes are all within a comparable temperature range between 56–64 °C. The data show that the length of the DNA seems to play an inferior role in the assembly process, thus providing variability in the sequence design of vesicular constructs as described herein.

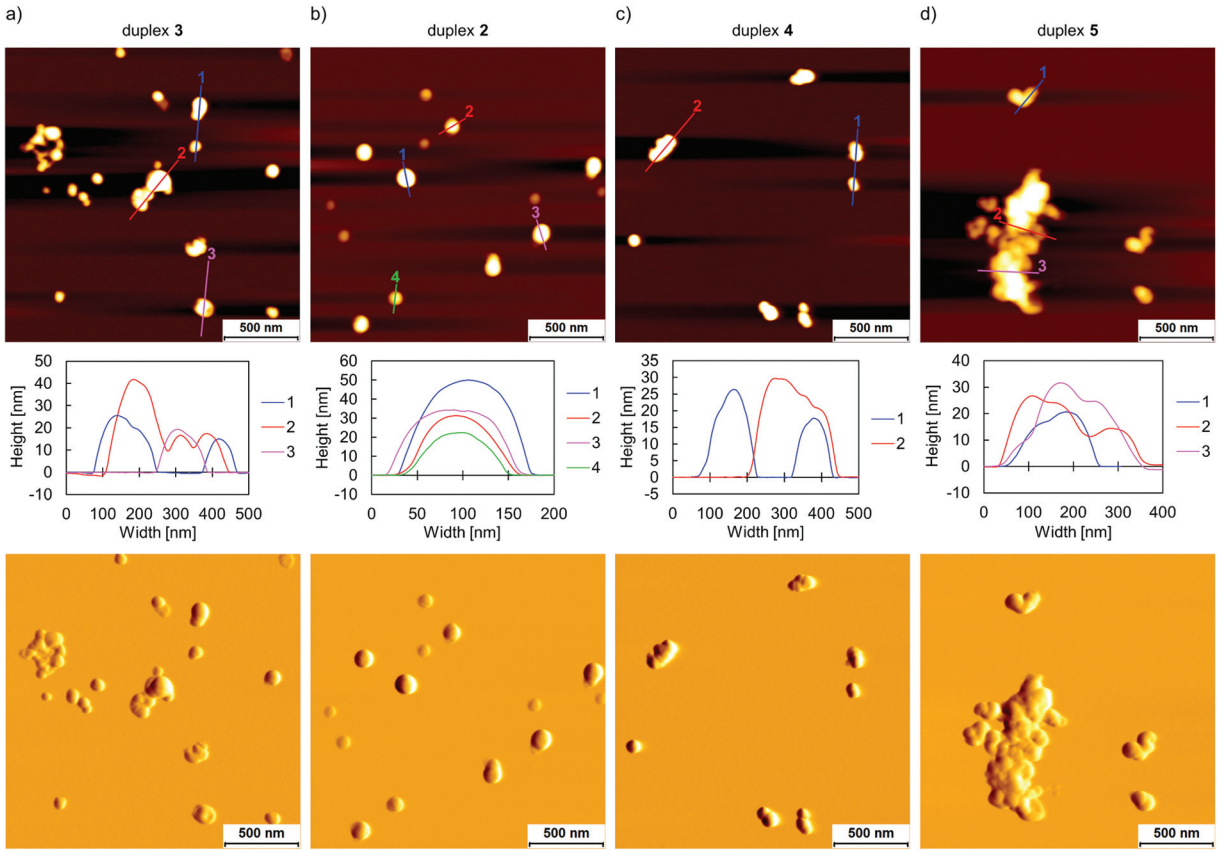

Fig. 3 AFM images incl. corresponding cross sections (top two rows) and deflection scans (bottom row) of self-assembled duplexes **3** (a), **2** (b), **4** (c), and **5** (d) after thermal assembly process (0.5 °C min^{-1}) on APTES-modified mica. Conditions: 1 μM each strand, 10 mM sodium phosphate buffer pH 7.2, 0.1 mM spermine·4 HCl, 20 vol% ethanol. APTES: (3-aminopropyl)triethoxysilane.

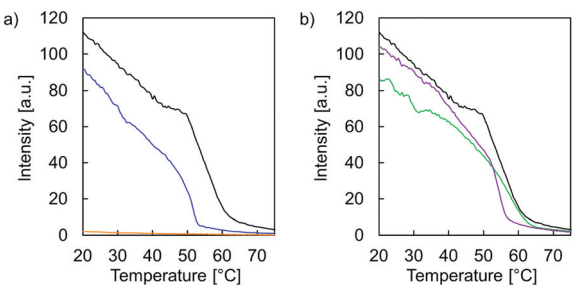

Fig. 4 Fluorescence-monitored annealing curves. (a) Black: **3**, blue: **2**, orange: **1**. (b) Black: **3**, green: **4**, purple: **5**. Conditions: 1 μM each strand, 10 mM sodium phosphate buffer pH 7.2, 0.1 mM spermine·4 HCl, 20 vol% ethanol, $\lambda_{ex.}$: 335 nm, $\lambda_{em.}$: 490 nm, gradient: 0.5 °C min^{-1}.

Table 1 Summary of nucleation temperatures and morphologies observed by AFM

DNA duplex	T_{FL}(nucleation)[a] [°C]	Morphology
1	—	No aggregates
2	53	Single vesicles
3	60–62	Agglomerated vesicles
4	62–64	Agglomerated vesicles
5	56	Agglomerated vesicles

[a] Determined by the onset temperature of the fluorescence-monitored annealing curve.

Vesicular constructs assembled from duplex **3** were further explored by cryo-EM imaging. The cryo-EM image presented in Fig. 5 confirms the vesicular morphology of the self-assemblies. The size of these vesicles ranges roughly between 140–200 nm in diameter. A distinct characteristic of the observed nanostructures is the presence of regular patterns. The inset in Fig. 5a reveals a rod-like pattern with a measured distance of 2.4 ± 0.5 nm between these rods.[49,50] Such a distance correlates well with the width of a single DNA duplex. Perpendicular to the rods, a defined membrane is apparent, with a thickness of 10.5 ± 0.6 nm (indicated by the yellow mark in the inset of Fig. 5a). This distance agrees with the length of duplex **3**. Considering these two distinct features, it is assumed that the vesicles are constructed by a core membrane with a columnar DNA duplex alignment, as illustrated in Fig. 5b. This core membrane is surrounded by one or more additional membranes. In these outer membrane(s), a pattern with darker bands is often present that corresponds to the length of duplex **3** and indicates an extended DNA arrangement (8.0 ± 0.5 nm, Fig. 5). Overall, cryo-EM imaging suggests vesicular constructs as displayed in Fig. 5b, which exhibit a

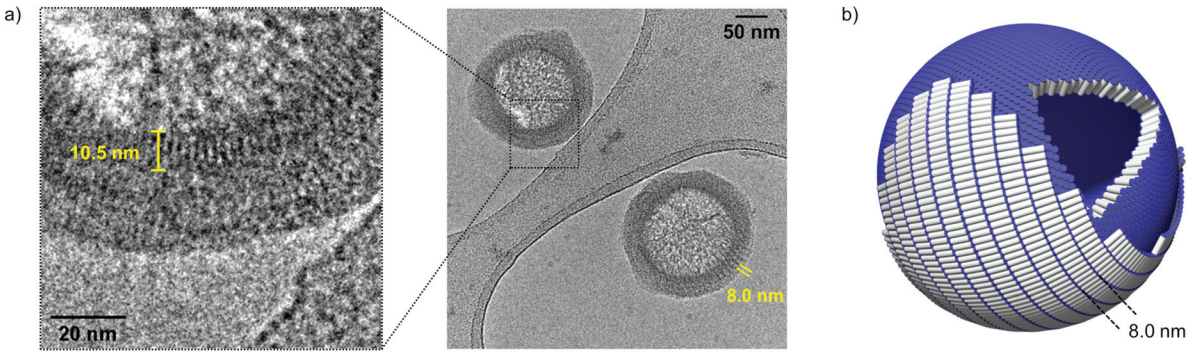

Fig. 5 (a) Cryo-EM image of self-assembled duplex **3**. (b) Schematic representation of vesicular construct assembled from duplex **3**. Duplexes **3** are represented as cylinders, with the DNA part in light gray and the TPE sticky ends in blue. For clarity, membranes are displayed partially only.

compact inner membrane and an outer membrane with an extended DNA duplex alignment. Additional cryo-EM images are provided in Fig. S18, ESI†.

In conclusion, the influence of the oligonucleotide design of 3′-/5′-end modified TPE–DNA conjugates on the supramolecular assembly behavior has been demonstrated. Varying the number of TPE units in the overhangs of the conjugates showed a substantial effect on the nucleation temperature obtained from fluorescence-monitored annealing curves. When extending the length of the sticky ends, a raise in the nucleation temperature is observed that is ascribed to increased hydrophobic interactions between the TPE residues. It was found that a minimum number of 2 TPE units per sticky end is required for the construction of nanostructures of this kind. Conversely, only a minor effect on the nucleation temperature was observed when the length of the DNA part within the oligonucleotides was varied. Cryo-EM imaging indicates that the vesicles are constructed from two individual types of membranes, that differ in their DNA duplex arrangement. Overall, this study contributes to a deliberate oligonucleotide design of 3′-/5′-end modified TPE–DNA conjugates for the successful supramolecular assembly into nanostructures. Ongoing research is directed towards the elaboration of novel types of DNA-based, functionalized architectures for nanotechnology applications. The presented design of the conjugates offers the possibility to introduce diverse types of tailored functionalization to the single-stranded complements of the TPE–DNA conjugates. Introduction of functionalities, such as polyethylene glycol chains or carbohydrate moieties, may lead to constructs for pharmacologically relevant applications.

Conflicts of interest

There are no conflicts to declare.

Acknowledgements

Financial support by the Swiss National Foundation (200020_188468 to R.H. and 31003A_179520 to B.Z.) is gratefully acknowledged. Cryo-electron microscopy was performed on equipment supported by the Microscopy Imaging Center (MIC), University of Bern, Switzerland.

References

1 N. C. Seeman and H. F. Sleiman, *Nat. Rev. Mater.*, 2017, **3**, 17068.
2 Y.-J. Chen, B. Groves, R. A. Muscat and G. Seelig, *Nat. Nanotechnol.*, 2015, **10**, 748–760.
3 E. Krieg, M. M. C. Bastings, P. Besenius and B. Rybtchinski, *Chem. Rev.*, 2016, **116**, 2414–2477.
4 D. Liu, S. H. Park, J. H. Reif and T. H. LaBean, *Proc. Natl. Acad. Sci. U. S. A.*, 2004, **101**, 717–722.
5 M. Walczak, R. A. Brady, L. Mancini, C. Contini, R. Rubio-Sánchez, W. T. Kaufhold, P. Cicuta and L. Di Michele, *Nat. Commun.*, 2021, **12**, 4743.
6 G. Fabrini, A. Minard, R. A. Brady, M. Di Antonio and L. Di Michele, *Nano Lett.*, 2022, **22**, 602–611.
7 H. Jun, X. Wang, M. F. Parsons, W. P. Bricker, T. John, S. Li, S. Jackson, W. Chiu and M. Bathe, *Nucleic Acids Res.*, 2021, **49**, 10265–10274.
8 N. A. Simeth, S. Kobayashi, P. Kobauri, S. Crespi, W. Szymanski, K. Nakatani, C. Dohno and B. L. Feringa, *Chem. Sci.*, 2021, **12**, 9207–9220.
9 P. W. K. Rothemund, *Nature*, 2006, **440**, 297–302.
10 H. Ramezani and H. Dietz, *Nat. Rev. Genet.*, 2020, **21**, 5–26.
11 R. P. Thomsen, M. G. Malle, A. H. Okholm, S. Krishnan, S. S. R. Bohr, R. S. Sørensen, O. Ries, S. Vogel, F. C. Simmel, N. S. Hatzakis and J. Kjems, *Nat. Commun.*, 2019, **10**, 5655.
12 J. R. Burns, E. Stulz and S. Howorka, *Nano Lett.*, 2013, **13**, 2351–2356.
13 J. Schill, B. J. H. M. Rosier, B. G. Audenis, E. M. Estirado, T. F. A. de Greef and L. Brunsveld, *Angew. Chem. Int. Ed.*, 2021, **60**, 7612–7616.
14 N. C. Seeman, *Nature*, 2003, **421**, 427–431.
15 J. Chen and N. C. Seeman, *Nature*, 1991, **350**, 631–633.
16 N. C. Seeman, *DNA Cell Biol.*, 1991, **10**, 475–486.

17 Y. P. Ohayon, C. Hernandez, A. R. Chandrasekaran, X. Wang, H. O. Abdallah, M. A. Jong, M. G. Mohsen, R. Sha, J. J. Birktoft, P. S. Lukeman, P. M. Chaikin, S. L. Ginell, C. Mao and N. C. Seeman, *ACS Nano*, 2019, **13**, 7957–7965.
18 M. Madsen and K. V. Gothelf, *Chem. Rev.*, 2019, **119**, 6384–6458.
19 M. Wolfrum, R. J. Schwarz, M. Schwarz, M. Kramer and C. Richert, *Nanoscale*, 2019, **11**, 14921–14928.
20 M. Nerantzaki, C. Loth and J.-F. Lutz, *Polym. Chem.*, 2021, **12**, 3498–3509.
21 T. MacCulloch, A. Buchberger and N. Stephanopoulos, *Org. Biomol. Chem.*, 2019, **17**, 1668–1682.
22 J. H. Yum, S. Park, R. Hiraga, I. Okamura, S. Notsu and H. Sugiyama, *Org. Biomol. Chem.*, 2019, **17**, 2548–2553.
23 N. Bürki, E. Grossenbacher, A. Cannizzo, T. Feurer, S. M. Langenegger and R. Häner, *Org. Biomol. Chem.*, 2020, **18**, 6818–6822.
24 G. Marth, A. M. Hartley, S. C. Reddington, L. L. Sargisson, M. Parcollet, K. E. Dunn, D. D. Jones and E. Stulz, *ACS Nano*, 2017, **11**, 5003–5010.
25 A. S. Gouda, Ł. Przypis, K. Walczak, P. T. Jørgensen and J. Wengel, *Org. Biomol. Chem.*, 2020, **18**, 6935–6948.
26 N. Appukutti, J. R. Jones and C. J. Serpell, *Chem. Commun.*, 2020, **56**, 5307–5310.
27 K. Pérez De Carvasal, N. Aissaoui, G. Vergoten, G. Bellot, J. J. Vasseur, M. Smietana and F. Morvan, *Chem. Commun.*, 2021, **57**, 4130–4133.
28 S. Benizri, A. Gissot, A. Martin, B. Vialet, M. W. Grinstaff and P. Barthélémy, *Bioconjugate Chem.*, 2019, **30**, 366–383.
29 S. P. W. Wijnands, E. W. Meijer and M. Merkx, *Bioconjugate Chem.*, 2019, **30**, 1905–1914.
30 M. Vybornyi, Y. Vyborna and R. Häner, *Chem. Soc. Rev.*, 2019, **48**, 4347–4360.
31 J. F. Lutz, J. M. Lehn, E. W. Meijer and K. Matyjaszewski, *Nat. Rev. Mater.*, 2016, **1**, 16024.
32 H. Bui, S. A. Díaz, J. Fontana, M. Chiriboga, R. Veneziano and I. L. Medintz, *Adv. Opt. Mater.*, 2019, **7**, 1900562.
33 L. Markova, M. Probst and R. Häner, *RSC Adv.*, 2020, **10**, 44841–44845.
34 C. Gong, S. Sun, Y. Zhang, L. Sun, Z. Su, A. Wu and G. Wei, *Nanoscale*, 2019, **11**, 4147–4182.
35 E. M. Estirado, A. F. Mason, M. Á. A. García, J. C. M. van Hest and L. Brunsveld, *J. Am. Chem. Soc.*, 2020, **142**, 9106–9111.
36 R. Kainuma, Y. Motohashi, T. Nishihara, R. Kurihara and K. Tanabe, *Org. Biomol. Chem.*, 2020, **18**, 5406–5413.
37 X. Wang, R. Sha, W. B. Knowlton, N. C. Seeman, J. W. Canary and B. Yurke, *ACS Nano*, 2022, **16**, 1301–1307.
38 C. D. Bösch, J. Jevric, N. Bürki, M. Probst, S. M. Langenegger and R. Häner, *Bioconjugate Chem.*, 2018, **29**, 1505–1509.
39 S. Rothenbühler, I. Iacovache, S. M. Langenegger, B. Zuber and R. Häner, *Nanoscale*, 2020, **12**, 21118–21123.
40 J. Luo, Z. Xie, J. W. Y. Lam, L. Cheng, H. Chen, C. Qiu, H. S. Kwok, X. Zhan, Y. Liu, D. Zhu and B. Z. Tang, *Chem. Commun.*, 2001, 1740–1741.
41 J. Li, J. Wang, H. Li, N. Song, D. Wang and B. Z. Tang, *Chem. Soc. Rev.*, 2020, **49**, 1144–1172.
42 X. Min, T. Fang, L. Li, C. Li, Z.-P. Zhang, X.-E. Zhang and F. Li, *Nanoscale*, 2020, **12**, 2340–2344.
43 S. Li, S. M. Langenegger and R. Häner, *Chem. Commun.*, 2013, **49**, 5835–5837.
44 J. Jing, Y.-R. Xue, Y.-X. Liu, B. Xu, H.-W. Li, L. Liu, Y. Wu and W. Tian, *Nanoscale*, 2020, **12**, 5501–5506.
45 W. Zhang, Z. Zhai, S. Li, X. Lin, W. Bai, N. Ding, Y. Zhang, J. Tong, J. Sun and C. Gao, *Nanoscale*, 2021, **13**, 138–149.
46 S. K. Saraswathi, V. Karunakaran, K. K. Maiti and J. Joseph, *Front. Chem.*, 2021, **9**, 716771.
47 J. Rong, Y. He, J. Tang, R. Qiao and S. Lin, *Nanoscale*, 2021, **13**, 5954–5964.
48 H. Ucar and H.-A. Wagenknecht, *Chem. Sci.*, 2021, **12**, 10048–10053.
49 J. Schindelin, I. Arganda-Carreras, E. Frise, V. Kaynig, M. Longair, T. Pietzsch, S. Preibisch, C. Rueden, S. Saalfeld, B. Schmid, J.-Y. Tinevez, D. J. White, V. Hartenstein, K. Eliceiri, P. Tomancak and A. Cardona, *Nat. Methods*, 2012, **9**, 676–682.
50 M. Linkert, C. T. Rueden, C. Allan, J.-M. Burel, W. Moore, A. Patterson, B. Loranger, J. Moore, C. Neves, D. MacDonald, A. Tarkowska, C. Sticco, E. Hill, M. Rossner, K. W. Eliceiri and J. R. Swedlow, *J. Cell Biol.*, 2010, **189**, 777–782.